Characterization of Cobalt-60 as a Nuclear Orientation Thermometer Source

C. M. Doyle[1,*] and T. O'Donnell[2]

[1] *Department of Physics, Seton Hall University, South Orange, NJ 07079*
[2] *Department of Physics, Virginia Polytechnic Institute and State University, Blacksburg, VA 24061*

(Dated: August 1, 2025)

Nuclear orientation thermometers exploit the angular asymmetry in gamma ray emission that can occur when an appropriately prepared gamma ray source is cooled to millikelvin temperatures. Here we report on the characterization of such a thermometer, which is based on embedded cobalt-60 nuclei in a hexagonal close packed cobalt single crystal. The characterization was carried out in the temperature range of 10-60 mK in a 3He-4He dilution refrigerator, and we studied differences in the intensities of gamma radiation measured by high purity germanium detectors placed on-axis and 90 degrees off-axis with respect to the angle of orientation of cobalt-60 nuclei. We characterized the magnitude of the anisotropy versus temperature values, which were measured by a ruthenium (IV) oxide thermometer, to assess if this sample exhibits the expected temperature-dependent behavior.

I. INTRODUCTION

The isotropic emission of gamma rays is a feature of cobalt-60 under certain temperature conditions. This phenomenon is characterized by the even and equal emission of gamma rays in all angular directions. No angle, or direction, is favored under these conditions, and there is a spherically symmetric pattern of gamma radiation being emitted from the source. When the temperature is high enough, the gamma rays being emitted by this isotope have a symmetry across all Zeeman levels and are evenly shared in terms of the levels they occupy. Detectors should detect gamma radiation equally, independent of the angle of detection from the source. At colder temperatures extending into the millikelvin range, however, an angular asymmetry arises in the emission of gamma rays by cobalt-60. As the crystal cools, it magnetizes, and the alignment of the nuclei with the magnetic field is referred to as nuclear orientation. Splitting of energy levels due to the interaction between the magnetic field and the magnetic moment of the nuclei occurs. Lower energy Zeeman levels become preferentially occupied, and so the relative population probabilities of each level are no longer equal [1]. This paper seeks to characterize a specifically prepared cobalt-60 sample for nuclear orientation thermometry. The characterization of the evolution of gamma ray asymmetry involves the use of resistive thermometry and the temperature measurements taken throughout this project are based on the readings of this kind of thermometer.

To prepare the sample, a hexagonal close packed single crystal was purchased from Goodfellow Corp. It was 1x1 mm on its face and 10 mm long. The crystal was grown so that the 001 axis, or the easy magnetization axis, pointed along the long dimension of the crystal. A sample of cobalt-59 was exposed to a thermal neutron beam to produce cobalt-60. This was done at the PULSTAR Reactor at North Carolina State University, and this reactor is shown in Figure 1.

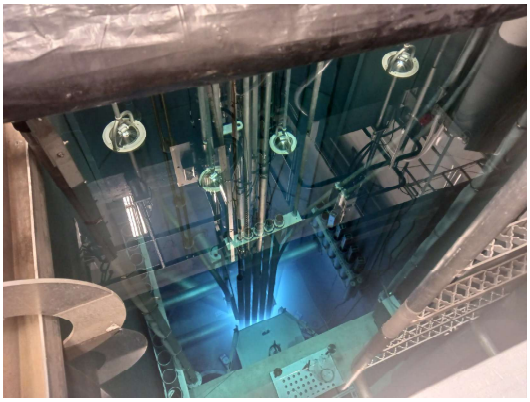

Figure 1. Reactor used in the process of producing a cobalt-60 sample.

The assessment of the performance of cobalt-60 in this paper relies closely on the accuracy of the resistive thermometer in relation to the true temperature of the cobalt-60 sample, which sits in a dilution fridge, embedded within a single crystal of cobalt with a hexagonal close packed structure. It is expected that, through an examination of the rates of detection of two perpendicular high purity germanium detectors, we will be able to gauge the temperature ranges at which the aforementioned anisotropy occurs. The point at which the thermometer loses sensitivity will also be of note, as this is the point where the lowest energy state dominates and anisotropy can no longer be measured as temperatures drop.

II. METHODS AND THEORY

Important parameters in our analysis are the yield, rate, and intensity, which we define here. The yield Y, or a measurement of the area under the gaussian fit applied to a gamma ray emission peak, must first be obtained before the rate can be calculated, which is defined as the

* Corresponding Author; doylecol@shu.edu

yield divided by the livetime of the run t. These two measurements are important in determining the overall intensity, W, of gamma ray detection in any particular detector, which we define as the rate of detection normalized to the rate of detection at high temperatures (R_h) [2], or $W = \frac{R}{R_h}$ where $R = \frac{Y}{t}$.

The theoretical prediction for intensity can also be expressed as a function that is dependent on both temperature and the angle of detection, as outlined in Ref. [1].

$$W(T,\theta) = 1 + \sum_{k=2,4} Q_k U_k F_k B_k(T) P_k(\cos\theta) \tag{1}$$

The variables in this equation are defined below. $B_k(T)$ is defined as the population of nuclear magnetic sublevels and therefore has a temperature dependence. It is defined as the following in Ref. [2].

$$B_k = I^k \frac{(2k)!}{(k!)^2} \sqrt{\frac{(2I+1)(2k+1)(2I-k)!}{(2I+k+1)!}} f_k(I) \tag{2}$$

The variable I represents the spin number of cobalt-60, which is equal to 5 [1]. As shown in equation (1), we will be summing over two values of k, where $k = 2$ and $k = 4$. The temperature dependence of $B_k(T)$ is made more evident once we express the following definition of $I^k f_k(I)$ when $k = 2$ and $k = 4$, as found in Ref. [1].

$$I^2 f_2(I) = \sum_{m=-I}^{+I} m^2 P(m) - \frac{I(I+1)}{3} \tag{3}$$

$$I^4 f_4(I) = \sum_{m=-I}^{+I} m^4 P(m) - a f_2 - b \tag{4}$$

where $a = \frac{I^2(6I^2+6I-5)}{7}$ and $b = \frac{(3I^2+3I-1)I(I+1)}{15}$.

$P(m)$ is the Boltzmann population probability when the magnetic sublevel is equal to m. k_B is the Boltzmann constant. This part of the equation is where the temperature dependence arises, as shown here, from Ref. [2].

$$P(m) = \frac{e^{-\epsilon_m/k_B T}}{\sum_{m=-I}^{+I} e^{-\epsilon_m/k_B T}} \tag{5}$$

$P_k(\cos\theta)$ represents the Legendre polynomials associated with $k = 2$ and $k = 4$ [3].

$$P_2(\cos\theta) = \frac{1}{2}(3\cos^2\theta - 1) \tag{6}$$

$$P_4(\cos\theta) = \frac{1}{8}(35\cos^4\theta - 30\cos^2\theta + 3) \tag{7}$$

The combined product of U_k and F_k are known for cobalt-60 [2], while the Q_k factor in the summation is experimentally determined and is a consequence of experimental design implementations [1].

By using this equation with temperature measurements from the resistive thermometer, we can compare theoretical values of intensity with measured intensity values. Anisotropy, denoted here as ξ, is defined in Ref. [4] as the following.

$$\xi = \frac{W(\pi/2) - W(0)}{W(\pi/2)} \tag{8}$$

As discussed earlier, high purity germanium detectors were used to measure the rate. Cooling techniques were used in order to heighten the sensitivity of detectors to gamma radiation [5], and in this experimental layout, both liquid nitrogen and mechanical cooling were utilized. These detectors were then positioned so that they were orthogonal to each other, with one lying on the angle of orientation of the nuclei, or on-axis, and the other placed at an angle of 90^o clockwise. These positions were chosen because intensity is a maximum and minimum at 90^o and 0^o respectively.

Both detectors were measured to stand at a vertical height of 56 inches from the ground, as this was the height of the cobalt-60 source within the fridge. Detector stands were constructed, assembled, and modified so as to mitigate height differences between detectors. A diagram of the experimental setup is as follows.

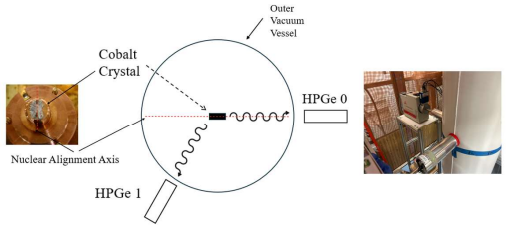

Figure 2. Diagram of the experimental layout and the relative positions of the cobalt-60 source, the nuclear alignment axis, and the outer vacuum vessel, which surrounds the dilution fridge. HPGe 1, contrary to this diagram, stood 90^o clockwise from HPGe 0.

The cobalt-60 source was kept in cryogenic conditions within a 3He-4He dilution fridge, in which a pulse tube and compressor acted on the helium through cyclic compressions and expansions, which gradually cooled the helium to temperatures reaching approximately 4 K. The lowering of the system to 4 K is essential to maintaining the dilution cycle of helium-3 and helium-4, and it is the expulsion of gaseous helium through a Joule-Thomson valve that causes the liquefaction of the helium. This process exploits the Joule-Thomson effect, which predicts the cooling of the temperature of gaseous particles during expansion, as well as increases in temperature during compression.

Cooling at the lowest temperature stage occurs when a small amount of helium-3 moves into a mixture containing mostly helium-4 [5]. The helium-3 is moved out of what is called the still, and into the mixing chamber, which contains mostly helium-4, as shown in Figure 3.

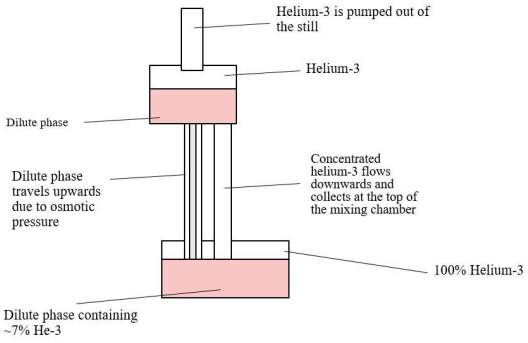

Figure 3. Diagram of the helium-3 and helium-4 dilution fridge.

Osmotic pressure develops when the balance between concentrations of helium-3 in the still and mixing chamber are altered. Pumping helium-3 away from the still allows for osmotic pressure to develop, leading cold helium-3 in the mixing chamber to flow upwards into the still in order to maintain a balance. This upward flow of colder helium-3 in a layer of outer tubing then cools the downward flow of warmer helium-3 in an inner layer of tubing.

Data was collected from the germanium detectors using a DT5780 CAEN MCA. Data analysis involved the setting of calibration points in CoMPASS, a software that allows for the analysis of emission spectra. After calibration points for the 1173.228 keV and the 1332.492 keV emission lines were set, the energy calibration was applied to the collected data. This allowed for the conversion of ADC counts to keV. We verified the calibration by using a background gamma ray from potassium-40. In subsequent runs, the peak that was measured at 1173 keV was then analyzed to assess the asymmetry's dependence on temperature.

Heat was applied to the mixing chamber to scan between temperatures ranging from 60 mK to 10 mK in steps of ~ 2 mK. The system was held at each step for approximately one hour.

The gaussian fit was set in order to calculate the centroid of the peak, as well as the yield. After graphing rate vs. temperature, as shown in Figure 4, we noticed clear differences in the rate measurements of the two detectors. The difference in the evolution of the rates of the two detectors was evidence of preferential emission of gamma radiation in the direction of the off-axis detector.

III. RESULTS AND ANALYSIS

The observed yields, rates, and intensities were analyzed as a function of their temperature dependence. The on-axis detector having decreasing rate measurements and the off-axis detector having increasing rate measurements, as temperatures dropped, thus demonstrating the temperature dependence of the angular asymmetries. The rate of the two detectors at high temperatures, however, were roughly the same, with the off-axis detector having a rate measurement of 15.75 counts/second and the on-axis detector having a rate measurement of 15.47 counts/second. The rate of the off-axis detector increased to approximately 17 counts/second while the rate of the on-axis detector decreased to approximately 13 counts/second at low temperatures. Measured intensity values were compared to values that were predicted using equation (1), and the following error propagation formula was used to determine the uncertainty of the measured intensities in the off-axis detector, with $\sigma_{R_h} = 0.07$ counts/second.

$$\sigma_{W_0} = W_0 \sqrt{\frac{{\sigma_R}^2}{R} + \frac{{\sigma_{R_h}}^2}{15.47}} \tag{9}$$

Similarly, the uncertainty of the measured intensity of the on-axis detector was calculated as follows.

$$\sigma_{W_{\frac{\pi}{2}}} = W_{\frac{\pi}{2}} \sqrt{\frac{{\sigma_R}^2}{R} + \frac{{\sigma_{R_h}}^2}{15.75}} \tag{10}$$

The anisotropy as it relates to drops in temperature can be mapped, with its uncertainties being accounted for by the following error propagation.

$$\sigma_A = \frac{W_0}{W_{\frac{\pi}{2}}} \sqrt{\frac{{\sigma_{W_{\frac{\pi}{2}}}}^2}{W_{\frac{\pi}{2}}} + \frac{{\sigma_{W_0}}^2}{W_0}} \tag{11}$$

The evolution of the rates, intensities, and anisotropy versus temperature is shown in Figures 4, 5, and 6.

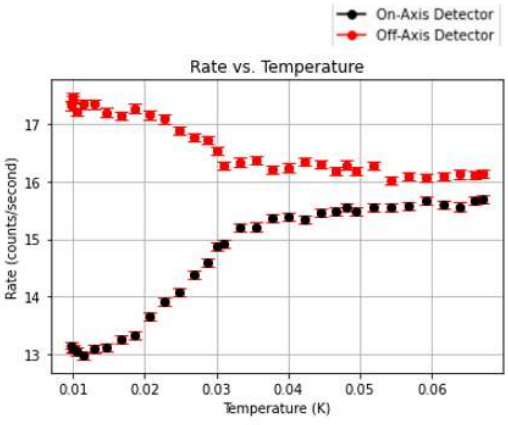

Figure 4. Measured rate in the on-axis and off-axis detectors versus temperature.

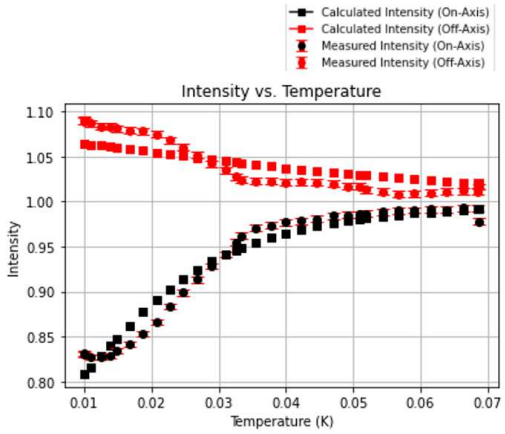

Figure 5. Calculated intensity values, as well as measured intensity values, versus temperature.

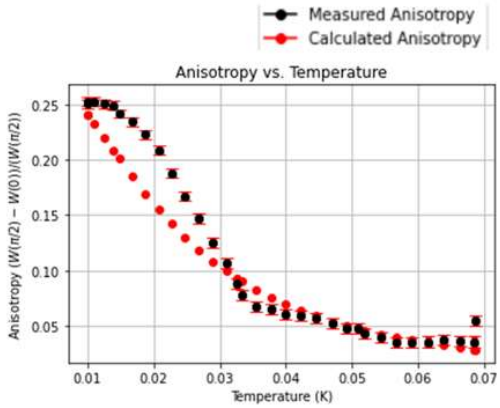

Figure 6. Calculated anisotropy values, as well as measured anisotropy values, versus temperature.

The geometry parameter, Q_k, was used to match the graphs of calculated values more closely to the graphs of the measured values as temperatures dropped. These geometry parameters differed from detector to detector, however, the magnetic field parameter was assumed to be constant since both detectors were used to measure gamma radiation from a common source. There is a plateauing that occurs in the graph of the measured intensities, and manipulation of the magnetic field value, through trial and error, helped to make sure that the plateauing of the calculated intensities matched more closely with the location at which it occurs in the experimental data. We used this process to estimate the magnetic field, which we found to be about 20 Tesla. The plateau, which is representative of the loss of sensitivity in the detectors to changes in temperature, was observed to occur at temperatures of approximately 15 mK. This occurs because the lowest energy state is dominant and no further change of anisotropy is expected.

IV. CONCLUSION

The temperature dependence of the angular asymmetry of gamma ray emission was evident in the graphs produced throughout the data analysis process. Results showed a loss of sensitivity at about 15 mK. While there is general agreement between the data and the theoretical expectation, better matching can be achieved through further analysis. For example, differences between the temperature of the resistive thermometer and the actual temperature of the radiation-emitting sample is one potential source of error. Self-heating may have been another source of error, as it has been noted in the literature that cobalt-60 has a steady state power dissipation of 0.57 nW per microCurie of β-emission [1], which can cause self-heating. The source used in this work had a radioactivity of about 1.8 μCi, or a power dissipation of approximately 1 nW.

Further work can focus on investigating the relationships of rate, intensity, and anisotropy versus temperature for detectors at different angular combinations. This work focused mainly on a detector placed on-axis, with another detector being positioned 90^o clockwise from the on-axis detector. Further work can characterize the temperature dependence at different angles, for example, by setting the detectors up so that we can include angular differences that increase in 30^o increments. This would be helpful in determining the extent to which this setup can be characterized in all directions, rather than simply in perpendicularly oriented detectors.

Other materials can also be used as the resistive thermometer, and an alternative to the method of gathering temperature data would be Speer carbon composition resistors, as this would be more sensitive than materials such as platinum-100 in the millikelvin range [6]. More investigation may seek to fully replace the ruthenium (IV) oxide thermometer or simply add a Speer carbon composition resistor as a secondary thermometer in the experimental design setup.

ACKNOWLEDGMENTS

I would like to thank my mentor, Dr. Thomas O'Donnell, for his guidance throughout the experimental setup and data analysis processes. ChatGPT was used as a syntax reference for data analysis code. We acknowledge support from NSF Grant No. PHY-2149165, the Department of Energy under Award No. DE-SC0020423 and the Virginia Tech Center for Neutrino Physics.

[1] F. Pobell, *Matter and Methods at Low Temperatures (3rd Edition)* (Springer, 2007).

[2] O. V. Lounasmaa, *Experimental Principles and Methods Below 1 K* (Academic Press, 1974).

[3] S. R. D. Groot *et al.*, Alpha-, Beta-, and Gamma-Ray Spectroscopy (Volume 2) (1968).
[4] H. Marshak, Journal of Research of the National Bureau of Standards (1983).
[5] N. H. Balshaw, *Practical Cryogenics* (Oxford Instruments, 2014).
[6] Y. Oda *et al.*, Cryogenics (Vol. 4, Iss. 2) (1974).